A model of interacting Navier-Stokes singularities

H Faller, D Geneste, B. Dubrulle

A model of interacting Navier-Stokes singularities

H. Faller[1], D. Geneste[1] and B. Dubrulle[1]
[1] *SPEC, CNRS UMR 3680, CEA, Université Paris-Saclay, 91190 Gif sur Yvette, France**
(Dated: March 29, 2021)

We introduce a model of interacting singularities of Navier-Stokes, named pinçons . They follow a Hamiltonian dynamics, obtained by the condition that the velocity field around these singularities obeys locally Navier-Stokes equations. This model can be seen of a generalization of the vorton model of Novikov[1], that was derived for the Euler equations. When immersed in a regular field, the pinçons are further transported and sheared by the regular field, while applying a stress onto the regular field, that becomes dominant at a scale that is smaller than the Kolmogorov length. We apply this model to compute the motion of a dipole of pinçons . When the initial relative orientation of the dipole is inside the interval $[0, \pi/2]$, a dipole made of pinçon of same intensity exhibits a transient collapse stage, following a scaling with dipole radius tending to 0 like $(t_c - t)^{0.63}$. For long time, the dynamics of the dipole is however repulsive, with both components running away from each other to infinity.

* hugues.faller@normalesup.org

I. INTRODUCTION

Snapshots of dissipation or enstrophy in turbulent fluids show us that small scales are intermittent, localized and irregular. Mathematical theorems constrain the degree of irregularity of such structures that are genuine singularities of the incompressible Navier-Stokes provided their spatial $\mathbb{L}^3$- norm is unbounded (for a review of various regularity criteria, see [2]). On the other hand, dissipation laws of turbulent flows suggest that they may be at most Hölder continuous with $h < 1/3$ [3] and of diverging vorticity in the inviscid limit. This observation has motivated several theoretical construction of turbulent Navier-Stokes small scale structures or weak solutions of Euler equations, using singular or quasi-singular entities based e.g. on atomic like structures [4], Beltrami flows [5], Mikado flows [6], spirals [7, 8] or vortex filaments [9].

These constructions have fueled a long-standing analytical framework of turbulence, allowing the modeling of proliferating and numerically greedy small scales by a countable (and hopefully numerically reasonable) number of degrees of freedom, provided by characteristics of the basic entities.

A good example of the possibilities offered by such a singular decomposition is provided by the 3D vorton description of Novikov [1]. In this model, the vorticity field is decomposed into N discretized singularities infinitely localized (via a δ function) at points r_α, $(\alpha = 1...N)$, each characterized by a vector $\boldsymbol{\gamma}_\alpha$ providing the intensity and the axis of rotation of motions around such singularities. The singularities are not fixed, but move under the action of the velocity field and velocity strain induced by the other singularities, so as to respect conservation of circulation. Around the singularity, the velocity field is not of divergence free, so that the vortons are akin to hydrodynamical monopoles interacting at long-range through a potential decaying like $1/r^2$. The model was adapted to enable numerical simulations of interacting vorticity rings or filaments by considering a divergence-free generalization of the vortons [10]. Quite remarkably, the vorton model results in vortex reconnection, even though no viscosity is introduced in the numerical scheme [11]. Whether the effective viscosity is due to intense vortex stretching [12], or to properties of vortex alignment during reconnection [11] is still debated.

From a mathematical point of view, the vorton model cannot be considered as a fully satisfying description of singularities of Navier-Stokes, because it does not respect the scaling invariance of Navier-Stokes, which imposes that the velocity field should scale like $1/r$. Indeed, through the Biot-Savart law, we see that a Dirac vortex field induces a velocity scaling like $1/r^2$, where r is the distance to singularity.

Motivated by this observation, we introduce in this paper a modification of the vorton model, that allows both respect of scale invariance of the Navier-Stokes equations, and simple dynamical description of the evolution of the basic entities, herefater named pinçons .

After useful generalities (Section 2.a), we introduce the pinçon model (Section 2.b) and describe their properties in Section 2.c. We introduce the Hamiltonian dynamics of pinçons in Section 2.d and 2.e. We then solve the equations for the special case of a dipole in Section 2.f. A discussion follows in Section 3.

II. PINÇON MODEL

A. Useful preliminary generalities

In this work, we will be considering entities based on a class of vectorial fields $\mathbf{U}$ that share the following properties in the vicinity of the origin:

- they are homogeneous of degree -1, meaning that $\forall \lambda \in \mathbb{R}, \mathbf{U}(\lambda \mathbf{x}) = \mathbf{U}(\mathbf{x})/\lambda$;
- they obey the stationary Navier-Stokes equations everywhere except at the origin.

Specifically, we have in some distributional sense:

$$\begin{aligned} \nabla \cdot \mathbf{U} &= 0, \\ (\mathbf{U} \cdot \nabla)\mathbf{U} + \frac{\nabla p}{\rho} - \nu \Delta \mathbf{U} &= \nu^2 \delta(\mathbf{x}) \mathbf{F}, \end{aligned} \tag{1}$$

where $\mathbf{F}$ is a vector with given orientation $\mathbf{e}$ and magnitude F. The velocity field is irregular at the origin, but we can study its behaviour near the origin by introducing a suitable test function ψ that is spherically symmetric around

$\mathbf{v}_\alpha$	$\dot{\boldsymbol{\gamma}}_\alpha\partial_\gamma(\mathbf{v}_\alpha)$	$\dot{\mathbf{x}}_\alpha\partial_x\mathbf{v}_\alpha$	$(\mathbf{v}_\alpha\cdot\nabla)\mathbf{v}_\alpha$	$(\mathbf{v}_\alpha\cdot\nabla)\mathbf{v}_\mathrm{R}$	$(\mathbf{v}_\mathrm{R}\cdot\nabla)\mathbf{v}_\alpha$	$(\mathbf{v}_\mathrm{R}\cdot\nabla)\mathbf{v}_\mathrm{R}$
$1/\ell$	$1/\ell$	$1/\ell^2$	$1/\ell^3$	$1/\ell$	$1/\ell^2$	1

TABLE I. Order of the various terms appearing in equation 3 as a function of the filter length ℓ in the limit $\epsilon \to 0$.

$x = 0$, positive of unit integral and C^∞, and considering the regularizations

$$\begin{aligned}
\overline{\mathbf{U}}^\ell(\mathbf{y}) &= \int_{\|\mathbf{x}\|>\epsilon} \psi\left(\frac{\mathbf{y}-\mathbf{x}}{\ell}\right)\mathbf{U}(\mathbf{x})\frac{\mathrm{d}\mathbf{x}}{\ell^3},\\
\overline{\nabla\mathbf{U}}^\ell(\mathbf{y}) &= -\int_{\|\mathbf{x}\|>\epsilon} \nabla\psi\left(\frac{\mathbf{y}-\mathbf{x}}{\ell}\right)\mathbf{U}(\mathbf{x})\frac{\mathrm{d}\mathbf{x}}{\ell^3}\\
\overline{\nabla^2\mathbf{U}}^\ell(\mathbf{y}) &= \int_{\|\mathbf{x}\|>\epsilon} \nabla^2\psi\left(\frac{\mathbf{y}-\mathbf{x}}{\ell}\right)\mathbf{U}(\mathbf{x})\frac{\mathrm{d}\mathbf{x}}{\ell^3},
\end{aligned} \tag{2}$$

where ϵ and ℓ are small parameters. Applying the change of variable $\mathbf{z} = \ell\mathbf{x}$ and using homogeneity, we see that in the limit $\epsilon \to 0$, we have $\overline{\mathbf{U}}^\ell(0) = \mathcal{O}(\ell^{-1})$, $\overline{\nabla\mathbf{U}}^\ell(0) = \mathcal{O}(\ell^{-2})$ and $\overline{\nabla^2\mathbf{U}}^\ell(0) = \mathcal{O}(\ell^{-3})$. Now, we consider a solution of the shape $\mathbf{v}_\alpha = \mathbf{U}(\mathbf{x} - \mathbf{x}_\alpha(t))$ and $\mathbf{F} = F(\gamma(t))\mathbf{e}(\mathbf{t})$, where F is a prescribed function, and $\mathbf{x}_\alpha$, $\boldsymbol{\gamma} = \gamma\mathbf{e}$, two vectors that parametrize the field $\mathbf{v}_\alpha$ as a function of t. Our goal is to determine the equations of motion of $\mathbf{x}_\alpha$ and $\boldsymbol{\gamma}$ that are compatible with the properties of Navier-Stokes equations. We thus introduce $\mathbf{v} = \mathbf{v}_\mathrm{R} + \mathbf{v}_\alpha$, where $\mathbf{v}_\mathrm{R}$ is a velocity field that is regular at the origin, and we impose that $\mathbf{v}$ is a solution of Navier-Stokes locally around the singularity at $\mathbf{x}_\alpha$, i.e. that $\mathbf{v}$ is a solution of

$$\partial_t\overline{\mathbf{v}}^\ell(\mathbf{x}_\alpha) + \overline{(\mathbf{v}\cdot\nabla)\mathbf{v}}^\ell(\mathbf{x}_\alpha) + \frac{\overline{\nabla p}^\ell(\mathbf{x}_\alpha)}{\rho} - \nu\overline{\Delta\mathbf{v}}^\ell(\mathbf{x}_\alpha) = 0. \tag{3}$$

Decomposing the velocity field into its regular and irregular part, we see that Eq. (3) generates terms of various orders in ℓ, that scale according to Table 1. Note that since $\mathbf{v}_\mathrm{R}$ is a regular field, it scales like $\mathcal{O}(1)$, so do its derivatives. Collecting the different term we find that the l.h.s. of Eq. (3) is the sum of the following orders:

$$\mathcal{O}(1) \ : \partial_t\overline{\mathbf{v}_\mathrm{R}}^\ell + \overline{(\mathbf{v}_\mathrm{R}\cdot\nabla)\mathbf{v}_\mathrm{R}}^\ell + \frac{\nabla\overline{p_\mathrm{R}}^\ell}{\rho} - \nu\Delta\overline{\mathbf{v}_\mathrm{R}}^\ell \tag{4}$$

$$\mathcal{O}(1/\ell) : \dot{\boldsymbol{\gamma}}\boldsymbol{\nabla}_\gamma\overline{\mathbf{v}_\alpha}^\ell + \overline{(\mathbf{v}_\alpha\cdot\nabla)\mathbf{v}_\mathrm{R}}^\ell \tag{5}$$

$$\mathcal{O}(1/\ell^2): -\dot{\mathbf{x}}_\alpha\nabla_{\mathbf{x}_\alpha}\overline{\mathbf{v}_\alpha}^\ell + \overline{(\mathbf{v}_\mathrm{R}\cdot\nabla)\mathbf{v}_\alpha}^\ell \tag{6}$$

$$\mathcal{O}(1/\ell^3): \overline{(\mathbf{v}_\alpha\cdot\nabla)\mathbf{v}_\alpha}^\ell + \frac{\nabla\overline{p_\alpha}^\ell}{\rho} - \nu\Delta\overline{\mathbf{v}_\alpha}^\ell \tag{7}$$

Cancelling the $\mathcal{O}(1/\ell^2)$ provides a first condition as:

$$\dot{\mathbf{x}}_\alpha\nabla_{\mathbf{x}}\overline{\mathbf{v}_\alpha}^\ell = \overline{(\mathbf{v}_\mathrm{R}\cdot\nabla)\mathbf{v}_\alpha}^\ell. \tag{8}$$

Due to the regularity of $\mathbf{v}_\mathrm{R}$, we can write $\overline{(\mathbf{v}_\mathrm{R}\cdot\nabla)\mathbf{v}_\alpha}^\ell = \mathbf{v}_\mathrm{R}(\mathbf{x}_\alpha)\cdot\overline{\nabla\mathbf{v}_\alpha}^\ell$ for small enough ℓ and ϵ. Condition (8) is then satisfied providing:

$$\dot{\mathbf{x}}_\alpha = \mathbf{v}_\mathrm{R}(\mathbf{x}_\alpha). \tag{9}$$

Physically, this means that the singularity point is advected by the regular field surrounding it.

Cancelling the $\mathcal{O}(1/\ell)$ provides a second condition, as:

$$\dot{\boldsymbol{\gamma}}\overline{\nabla_\gamma\mathbf{v}_\alpha}^\ell = -\overline{(\mathbf{v}_\alpha\cdot\nabla)\mathbf{v}_\mathrm{R}}^\ell. \tag{10}$$

Due to the regularity of $\mathbf{v}_\mathrm{R}$, we can write $\overline{(\mathbf{v}_\alpha\cdot\nabla)\mathbf{v}_\mathrm{R}}^\ell = (\overline{\mathbf{v}_\alpha}^\ell\cdot\nabla)\mathbf{v}_\mathrm{R}(\mathbf{x}_\alpha)$. We then get the equation:

$$\dot{\boldsymbol{\gamma}}\overline{\nabla_\gamma\mathbf{v}_\alpha}^\ell = -(\overline{\mathbf{v}_\alpha}^\ell\cdot\nabla)\mathbf{v}_\mathrm{R}. \tag{11}$$

Physically, this means that the force axis and its direction are moved around by the shear of the regular field at the location of the singularity.

Taking finally into account Eq. (1), we are then left with the equation for $\mathbf{x}$ close to $\mathbf{x}_\alpha$:

$$\partial_t \overline{\mathbf{v}_\mathrm{R}}^\ell(\mathbf{x}) + (\overline{\mathbf{v}_\mathrm{R}}^\ell \cdot \nabla)\overline{\mathbf{v}_\mathrm{R}}^\ell(\mathbf{x}) + \frac{\nabla \overline{p_R}^\ell}{\rho}(\mathbf{x}) - \nu\Delta\overline{\mathbf{v}_\mathrm{R}}^\ell(\mathbf{x}) = \tau^\ell(\mathbf{x}) - \frac{\nu^2}{\ell^3}\psi\left(\frac{\mathbf{x}-\mathbf{x}_\alpha}{\ell}\right)\mathbf{F}, \tag{12}$$

where $\tau^\ell = \nabla \cdot \left(\overline{\mathbf{v}_\mathrm{R}}^\ell \overline{\mathbf{v}_\mathrm{R}}^\ell - \overline{\mathbf{v}_\mathrm{R}\mathbf{v}_\mathrm{R}}^\ell\right)$ is the Reynolds stress contribution due to filtering. Eq. (12) describes the back reaction of the singular part of the field onto the regular field through the force that it applies at the location of the singularity. Physically, this force appears as an extra "turbulent stress" that is due to the singularity and that adds to the normal filtering contribution to provoke "deviations from Navier-Stokes" equations. At large scale, this back reaction is negligible in front of the classical turbulent stress. The scale at which the two terms become of the same order of magnitude can be computed through the estimate: $\tau^\ell = \mathcal{O}(\delta\boldsymbol{v}_\ell^2/\ell)$ [13], where $\delta\boldsymbol{v}_\ell = \mathbf{v}_\mathrm{R}(\mathbf{x}+\ell) - \mathbf{v}_\mathrm{R}(\mathbf{x})$. Since $\mathbf{v}_\mathrm{R}$ is regular, it can be expanded as $\mathbf{v}_\mathrm{R}(\mathbf{x}+\ell) - \mathbf{v}_\mathrm{R}(\mathbf{x}) = \ell\nabla\mathbf{v}_\mathrm{R}$, so that $\tau^\ell \sim \ell(\nabla\mathbf{v}_\mathrm{R})^2$. It balances the contribution due to singularity at a scale such that $\nu^3/\ell^4 \sim \nu(\nabla\mathbf{v}_\mathrm{R})^2$. This corresponds then to $\ell = \eta_\mathrm{K}$, the Kolmogorov scale based on the dissipation of the regular field. Below such scale, the singularity is therefore providing the dominant contribution to the "turbulent stress". This means that by measuring velocity flows at resolution smaller than the Kolmogorov scale, we should be able to observe deviations from the Navier-Stokes equations, that do not converge to zero when increasing resolution.

This description is quite general, and independent of the details of the singularity. We now apply it to a specific solution to infer our pinçon model.

B. Definition of pinçon

We introduce the pinçons as individual entities labeled by α, characterized by their position $\mathbf{x}_\alpha(t)$, and a 4D vector $(p_\alpha(t), \boldsymbol{\gamma}_\alpha(t))$, with $\|\boldsymbol{\gamma}_\alpha\| < 1$, that produce locally an axisymmetric velocity field around the axis of direction $\boldsymbol{\gamma}_\alpha$ given by:

$$\mathbf{v}_\alpha(\mathbf{x}) = \frac{2}{\phi_\alpha}\left(\boldsymbol{\gamma}_\alpha - \frac{\mathbf{x}-\mathbf{x}_\alpha}{\|\mathbf{x}-\mathbf{x}_\alpha\|}\right) + 2(1-\boldsymbol{\gamma}_\alpha^2)\frac{\mathbf{x}-\mathbf{x}_\alpha}{\phi_\alpha^2}, \tag{13}$$

$$p_\alpha = -\frac{4}{\|\mathbf{x}-\mathbf{x}_\alpha\|\phi_\alpha} + 4\frac{1-\boldsymbol{\gamma}_\alpha^2}{\phi_\alpha^2}. \tag{14}$$

where $\phi(\mathbf{x},\boldsymbol{\gamma}) = \|\mathbf{x}\| - \boldsymbol{\gamma}\cdot\mathbf{x}$ and $\phi_\alpha = \phi(\mathbf{x}-\mathbf{x}_\alpha, \boldsymbol{\gamma}_\alpha)$. A few useful properties of ϕ are put in Appendix. In particular, the velocity field given by Eq. (13) is homogeneous of degree -1 around $\mathbf{x}_\alpha$, and axisymmetric around the direction of $\boldsymbol{\gamma}$. Plots of velocity and vorticity around a pinçon are displaid in figure 1. Close to the singularity, there is a neck pinch of the velocity streamlines, hence their name pinçon. As first shown by Landau [14] (see also [15–18]), the velocity fields $\mathbf{v}_\alpha$ are solutions of (1) with

$$\begin{aligned} \mathbf{F} &= F(\gamma)\frac{\boldsymbol{\gamma}_\alpha}{\gamma}, \\ F(\gamma) &= 4\pi\left[\frac{4}{\gamma} - \frac{2}{\gamma^2}\ln\left(\frac{1+\gamma}{1-\gamma}\right) + \frac{16}{3}\frac{\gamma}{1-\gamma^2}\right], \\ \gamma &= \|\boldsymbol{\gamma}_\alpha\|. \end{aligned} \tag{15}$$

We refer the reader to [17] for a rigorous derivation of such result. The function $F(\gamma)$ is shown in Fig. 2-a. It starts from 0 at $\gamma = 0$, with a linear behaviour $F(\gamma) = 16\pi\gamma$ near the origin, and diverges at $\gamma = 1$.

C. Properties of pinçons

1. *Potential vector, vorticity and helicity*

Using vector calculus identities, we can check that the velocity field around a pinçon derives from the vector potential:

$$\begin{aligned} \mathbf{A}_\alpha(\mathbf{x}) &= 2(\mathbf{x}-\mathbf{x}_\alpha)\times\nabla\ln(\phi_\alpha), \\ &= 2\frac{\boldsymbol{\gamma}_\alpha\times(\mathbf{x}-\mathbf{x}_\alpha)}{\phi_\alpha}, \end{aligned} \tag{16}$$

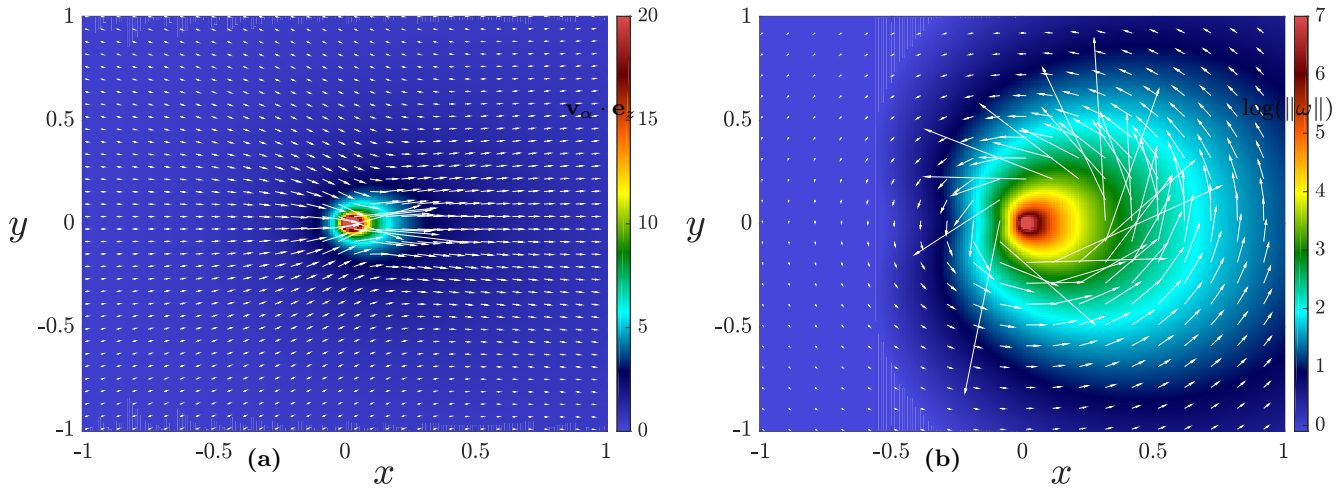

FIG. 1. (a) Velocity and (b) vorticity field around a pinçon . The white arrows provide the velocity and vorticity in the plane generated by $\mathbf{x}$ and $\boldsymbol{\gamma}_\alpha$. The colour codes the logarithm in base 10 of of the out of plane (vertical) velocity (a) and half the enstrophy (b).

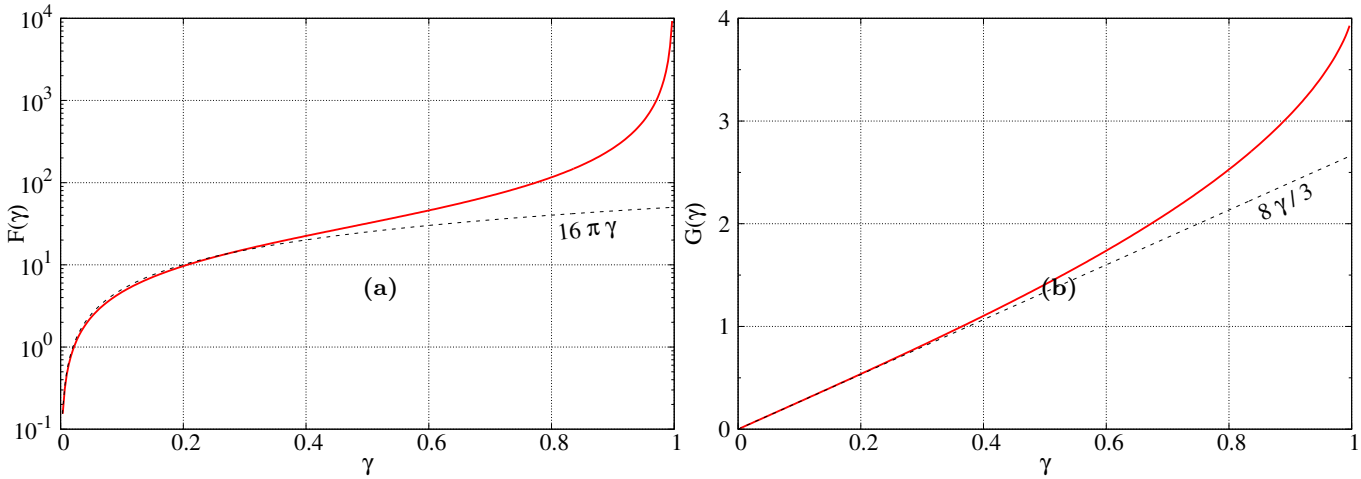

FIG. 2. Parameters of a pinçon as a function of its intensity γ. (a) Intensity of the force produced by the pinçon at its location. The black dashed line has equation $y = 16\pi\gamma$; (b) Generalized momentum of a pinçon . The black dashed line has equation $y = 8\gamma/3$.

We can formally define the vorticity field produced locally around a pinçon by taking the rotational of $\mathbf{v}_\alpha$. The vorticity is parallel to the potential vector and reads:

$$\boldsymbol{\omega}_\alpha(\mathbf{x}) = 4(1-\gamma^2)\frac{\boldsymbol{\gamma}_\alpha \times (\mathbf{x}-\mathbf{x}_\alpha)}{\phi_\alpha^3}, \tag{17}$$

From this, we see that the velocity field produced by a pinçon is of zero helicity.

2. *Generalized Momentum*

The velocity field diverges at the location of the pinçon so it is undefined as such point. We may however define a generalized momentum $\boldsymbol{\Pi}_\alpha$ for the pinçon by using the average of the velocity field over a sphere of unit radius (see

appendix for its computation):

$$\mathbf{\Pi}_\alpha = G(\gamma_\alpha)\frac{\boldsymbol{\gamma}_\alpha}{\gamma_\alpha},$$
$$G(\gamma) = \frac{2}{\gamma^2}\left[2\gamma - (1-\gamma^2)\ln\left(\frac{1+\gamma}{1-\gamma}\right)\right]. \tag{18}$$

By homogeneity, the average of the velocity over an arbitrary sphere of radius ℓ is simply $\langle \mathbf{v}_\alpha\rangle_{\mathcal{B}_\ell} = \mathbf{\Pi}_\alpha/\ell$. Note that $\mathbf{\Pi}_\alpha$ points in the direction of $\boldsymbol{\gamma}_\alpha$. For $0 \leq \gamma < 1$, $G(\gamma)$ varies smoothly from 0 to 4, starting from a linear behavior $G(\gamma) = 8\gamma/3$ at the origin and ending with a vertical tangent at $\gamma = 1$ (see Fig. 2-b). Therefore the function $G(\gamma)$ is bijective, and there is a one-to-one correspondance between G and γ and $\mathbf{\Pi}$ and $\boldsymbol{\gamma}$.

D. Interactions of pinçons

An ensemble of N pinçons , $\alpha = 1...N$ produces a velocity field $\mathbf{v}(x,t)$:

$$\mathbf{v}(x,t) = \sum_\alpha \mathbf{v}_\alpha(x,t), \tag{19}$$

Around a pinçon α, the ensemble of other pinçons produces a regular field $\mathbf{v}_{\mathrm{R}} = \sum_{\beta\neq\alpha}\mathbf{v}_\beta(\mathbf{x}_\alpha)$. Motivated by such observation, we introduce, for each pinçon , the Hamiltonian:

$$H_\alpha = \mathbf{\Pi}_\alpha \cdot \sum_{\beta\neq\alpha}\mathbf{v}_\beta(\mathbf{x}_\alpha,t), \tag{20}$$

and *define* the interaction of pinçons through the sets of $2N$ Hamiltonian equations:

$$\dot{\mathbf{x}}_\alpha = \frac{\delta H_\alpha}{\delta \mathbf{\Pi}_\alpha}, \tag{21}$$
$$\dot{\mathbf{\Pi}}_\alpha = -\frac{\delta H_\alpha}{\delta \mathbf{x}_\alpha}, \tag{22}$$

where the dot denotes the time derivative. Developing such expressions, we get the following set of $2N$ differential equations:

$$\dot{\mathbf{x}}_\alpha = \sum_{\beta\neq\alpha}\mathbf{v}_\beta(\mathbf{x}_\alpha,t), \tag{23}$$
$$\dot{\mathbf{\Pi}}_\alpha = -\mathbf{\Pi}_\alpha \cdot \sum_{\beta\neq\alpha}\nabla_{\mathbf{x}_\alpha}\mathbf{v}_\beta(\mathbf{x}_\alpha,t). \tag{24}$$

Since $\mathbf{\Pi}_\alpha$ is a function of $\boldsymbol{\gamma}_\alpha$, we can further write $\dot{\mathbf{\Pi}}_\alpha = \dot{\boldsymbol{\gamma}}_\alpha\nabla_{\boldsymbol{\gamma}_\alpha}\mathbf{\Pi}_\alpha$. Given $\mathbf{\Pi}_\alpha$ is the average of $\mathbf{v}_\alpha$ over any sphere of constant radius and taking into account the homogeneity, we see that the equations (24) correspond to the Eqs. (9) and (11), using an average over a sphere of radius ℓ such as $\langle X\rangle_{\mathcal{B}_\ell}$ instead of $\overline{X}^\ell$. Therefore, the equations of motions of the pinçons correspond to the equations that are imposed by the structure of the Navier-Stokes equations and the requirement that the local velocity field induced by each pinçon should obey such equations. In some sense, Eqs. 24 can therefore be seen as the equivalent of the motion of poles or zeros of partial differential equations that have been computed, starting from Kruskal[19] for the KdV equations (see [20, 21] for a review). Being Hamiltonian, the equations of the pinçons are characterized by N integral of motions, H_α $\alpha = 1...N$. The motions is furthermore constrained by imposing that the motions stay with the unit hypersphere such that $\|\boldsymbol{\gamma}_\alpha\| < 1$.

E. Weak pinçon limit

The Hamiltonian 20 takes a simple expression, in the "weak pinçon " limit, where the intensity of the pinçons are very small, $\gamma_\alpha \ll 1$ for any α. In this case, $\mathbf{\Pi}_\alpha = 8\boldsymbol{\gamma}_\alpha/3$ and one can develop $\phi^{-1}_{\alpha\beta} = (1 + \boldsymbol{\gamma}_\beta \cdot \mathbf{r}_{\alpha\beta}/\|\mathbf{r}_{\alpha\beta}\|)$. We then find .

$$H_\alpha = \frac{16}{3}\sum_{\beta\neq\alpha}\left[\frac{\boldsymbol{\gamma}_\alpha\cdot\boldsymbol{\gamma}_\beta}{\|\mathbf{r}_{\alpha\beta}\|} + \frac{(\boldsymbol{\gamma}_\alpha\cdot\mathbf{r}_{\alpha\beta})(\boldsymbol{\gamma}_\beta\cdot\mathbf{r}_{\alpha\beta})}{\|\mathbf{r}_{\alpha\beta}\|^3}\right], \tag{25}$$

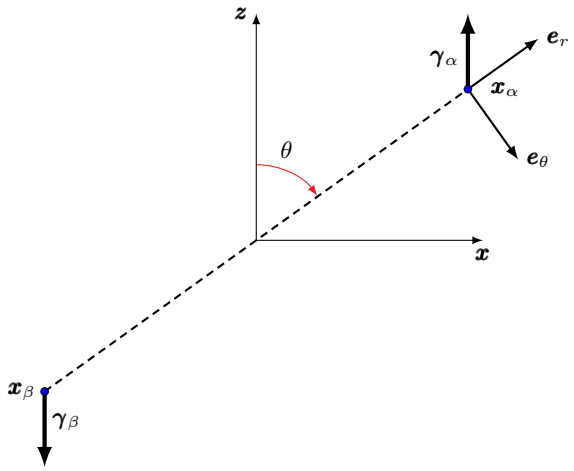

FIG. 3. Geometry of the dipole: two pinçons located at $\mathbf{x}_\alpha$ and $\mathbf{x}_\beta$, and such that initially $\boldsymbol{\gamma}_\alpha + \boldsymbol{\gamma}_\beta = 0$. By convention, the angle θ is the angle between $\boldsymbol{\gamma}_\alpha$ and $\mathbf{r} = \mathbf{x}_\alpha - \mathbf{x}_\beta$.

which is the classical self interaction energy of pair of singularities [12]. The equations of motions under such approximations are :

$$\begin{aligned}
\dot{\mathbf{x}}_\alpha &= 2 \sum_{\beta \neq \alpha} \left[\frac{\boldsymbol{\gamma}_\beta}{\|\mathbf{r}_{\alpha\beta}\|} + (\boldsymbol{\gamma}_\beta \cdot \mathbf{r}_{\alpha\beta}) \frac{\mathbf{r}_{\alpha\beta}}{\|\mathbf{r}_{\alpha\beta}\|^2} \right], \\
\dot{\boldsymbol{\gamma}}_\alpha &= 2 \sum_{\beta \neq \alpha} \left[(\boldsymbol{\gamma}_\alpha \cdot \boldsymbol{\gamma}_\beta) \frac{\mathbf{r}_{\alpha\beta}}{\|\mathbf{r}_{\alpha\beta}\|^3} + 3\,(\boldsymbol{\gamma}_\alpha \cdot \mathbf{r}_{\alpha\beta})(\boldsymbol{\gamma}_\beta \cdot \mathbf{r}_{\alpha\beta}) \frac{\mathbf{r}_{\alpha\beta}}{||\mathbf{r}_{\alpha\beta}||^5} \right. \\
&\quad \left. - \boldsymbol{\gamma}_\alpha \frac{\boldsymbol{\gamma}_\beta \cdot \mathbf{r}_{\alpha\beta}}{\|\mathbf{r}_{\alpha\beta}\|^3} - \boldsymbol{\gamma}_\beta \frac{\boldsymbol{\gamma}_\alpha \cdot \mathbf{r}_{\alpha\beta}}{\|\mathbf{r}_{\alpha\beta}\|^3} \right].
\end{aligned} \tag{26}$$

These equations of motions are reminiscent of the equations of motions of the vortons (see Eq. 41 in Appendix), with vectorial products being replaced by scalar product, and additional terms appearing. However, the motion and intensities of the pinçons are driven by forces decaying respectively like $1/r$ and $1/r^2$, rather than respectively $1/r^2$ and $1/r^3$ for the vortons.

Due to the symmetries, the two body interaction of two pinçons , say α and β exhibit interesting properties: indeed, the two integral of motions satisfy $H_\alpha = H_\beta$. Moreover, $\boldsymbol{r}_{\alpha\beta} = \ - \ \boldsymbol{r}_{\beta\alpha}$, so that $\dot{\boldsymbol{\gamma}}_\alpha = -\dot{\boldsymbol{\gamma}}_\beta$: the total momentum $\boldsymbol{\Gamma} \equiv \boldsymbol{\gamma}_\alpha + \boldsymbol{\gamma}_\beta$ is an additional constant of motion and is conserved during the interaction. Furthermore, the center of mass, located at $\mathbf{x}_\alpha + \mathbf{x}_\beta$, has a velocity given by:

$$\mathbf{V} \equiv \dot{\mathbf{x}}_\alpha + \dot{\mathbf{x}}_\beta = 2 \left[\frac{\boldsymbol{\Gamma}}{\|\mathbf{r}_{\alpha\beta}\|} + (\boldsymbol{\Gamma} \cdot \mathbf{r}_{\alpha\beta}) \frac{\mathbf{r}_{\alpha\beta}}{\|\mathbf{r}_{\alpha\beta}\|^2} \right]. \tag{27}$$

Therefore, whenever $\boldsymbol{\Gamma} \neq \mathbf{0}$, the center of mass accelerates to infinity (resp. decelerates to zero) whenever the two pinçons get close to each other (resp. separate from each other). This situation is reminiscent of the collapse of a 2D vortex dipole, with different scalings, due to the fact that the vortex Hamiltonian has interactions scaling like $\log(r)$ instead of $1/r$ here. The case with $\boldsymbol{\Gamma} = \mathbf{0}$ can actually be treated without approximation about the dipoles intensities, as we now show.

F. Dynamics of a dipole of pinçons

Let us consider the dynamics of a dipole, sketched in Figure 3, made of two pinçons located at $\mathbf{x}_\alpha$ and $\mathbf{x}_\beta$, and such that initially $\boldsymbol{\gamma}_\alpha + \boldsymbol{\gamma}_\beta = 0$. We have then $\mathbf{v}_\beta(\mathbf{x}_\alpha) = -\mathbf{v}_\alpha(\mathbf{x}_\beta) \equiv \mathbf{V}$ and $H_\alpha = H_\beta \equiv H$. Introducing further

$\mathbf{r} = \mathbf{x}_\alpha - \mathbf{x}_\beta$, we get the equation of motions:

$$\begin{aligned}
\dot{\mathbf{x}}_\alpha &= \mathbf{V}, \\
\dot{\mathbf{x}}_\beta &= -\mathbf{V}, \\
\dot{\mathbf{\Pi}}_\alpha &= -\nabla_r H, \\
\dot{\mathbf{\Pi}}_\beta &= \nabla_r H.
\end{aligned} \tag{28}$$

Therefore, the centre of mass of the dipole $\mathbf{x}_\alpha + \mathbf{x}_\beta$ does not move, while the total dipole strength $\mathbf{\Pi}_\alpha + \mathbf{\Pi}_\beta$ remains equal to 0: the dipole remains a dipole and both $\mathbf{\Pi}_\alpha = -\mathbf{\Pi}_\beta \equiv \mathbf{\Pi}$ and $\boldsymbol{\gamma}_\alpha = \ - \ \boldsymbol{\gamma}_\beta \equiv \boldsymbol{\gamma}$. The dipole dynamics of the quantities characterizing the dipole, namely $\mathbf{r}$ and $\boldsymbol{\gamma}$ (or equivalently $\mathbf{\Pi}$), can be obtain by taking the difference of the first two and the last two equations of Eq. 28 to get:

$$\dot{\mathbf{r}} = 4\left(-\frac{\boldsymbol{\gamma} + \mathbf{r}/r}{r\phi_*} + (1-\gamma^2)\frac{\mathbf{r}}{r^2\phi_*^2}\right), \tag{29}$$

$$\dot{\mathbf{\Pi}} = -2G(\gamma)\nabla_r\left(-\frac{\gamma + \cos(\theta)}{r\phi_*} + (1-\gamma^2)\frac{\cos(\theta)}{r\phi_*^2}\right), \tag{30}$$

where $r = \|\mathbf{r}\|$, $\cos(\theta) = (\boldsymbol{\gamma}\cdot\mathbf{r})/(r\gamma)$, $\phi_* = 1 + \gamma\cos(\theta)$ and $G(\gamma) = \|\mathbf{\Pi}\|$.

From these expressions, we see that the evolution of $\mathbf{r}$ and $\mathbf{\Pi}$ remains in the plane generated by the two vectors $\mathbf{r}$ and $\boldsymbol{\gamma}$. We are then left with only 3 independent quantities to determine the dipole axis and its orientation, namely r, θ and γ. The evolution of the first two quantities can be simply derived by projecting Eq. 29 on $\mathbf{e}_r$ and $\mathbf{e}_\theta$, while the last quantity can be obtained by using the fact that H is a constant of motion. We thus get after straightforward simplifications:

$$\dot{r} = \frac{4}{r}\left(\frac{1-\gamma^2}{\phi_*^2} - 1\right), \tag{31}$$

$$r\dot{\theta} = 4\,\frac{\gamma\sin\theta}{r\phi_*}, \tag{32}$$

$$H = 2\frac{G(\gamma)}{r}\left(-\frac{\gamma + \cos(\theta)}{\phi_*} + (1-\gamma^2)\frac{\cos(\theta)}{\phi_*^2}\right). \tag{33}$$

We have integrated the equations of motions (33) for fixed intial radius $r_0 = 1$ and $\gamma_0 = 0.5$ and various initial values of θ_0. The resulting evolutions are summarized in figure 4. We see that there are two fixed points of the dynamics for θ: one stable and attractive, corresponding to $\theta = \pi$, and one unstable and repulsive, corresponding to $\theta = 0$. As a result, the pinçons are mostly repulsing each other, except when they start exactly anti-aligned and facing away each other, in which case they attract each other and anihiliate each other. The pinçons that are initially in the interval $[\pi/2, \pi]$ run away from each other while increasing their strength continuously. The pinçons with initial inclinaison in the interval $[0, \pi/2]$ and different from 0 start moving towards each other, while decreasing their strength and increasing their angle, in absolute value. Once they reach the value $\theta = \pi/2$ (around $t \sim \frac{1}{4}$), they change direction and get away from each other (see figure 7-b). The collapse stage is nearly universal, with weak dependance on the initial angle (through e.g. the fitting parameter t_c), while the escape depends more strongly on the initial orientation. Such asymmetry has been also observed in reconnection of quantum vortices [22]. A more detailed investigation of the scaling laws for dipole separation is provided in figure 5. We have found that during the collapse stage, the radius of the dipole decreases like $(t_c - t)^{0.63}$ (which is steeper than the Leray scaling $\sqrt{t_c - t}$ [23]). During the separating stage, θ gets closer to π and the quantity $\frac{r^{1.24}}{t}$ remains constant at long times ($t \geq 2$), resulting in a power law escape law $r \sim t^{0.81}$.

During the interaction, the maximum velocity and vorticity near the dipole exhibit marked oscillations, due to subtil cancellations in between the contributions from the two poles. Using a moving average, we see however that during the collapse stage, they first decrease until the time of minimum of γ and r, after which they increase until the angle is close to $\theta = \pi$, then, they finally both decay to zero, see figure 6. Despite a different exponent, the behaviour is reminiscent of what is happening during a reconnection of vortex rings, where the distance between rings decay like $\sqrt{t_c - t}$, with maximum velocity and vorticity growing up then decaying [24]. Due to the Hamiltonian dynamics, the dipole dynamics remains into an hyperplan with equation $H = H(t = 0)$, see figure 7-a. Generically, the collapse of the dipole represent a dipole anihilation, since it disappears in a finite time (the intensity of its components going to 0). This is however only observed for interactions with initial angle $\theta = 0$. It would be interesting to conduct further simulations of N dipoles with different intensities, to see whether the annihilation process generically occurs more frequently after a number of interactions. We leave this question for further work.

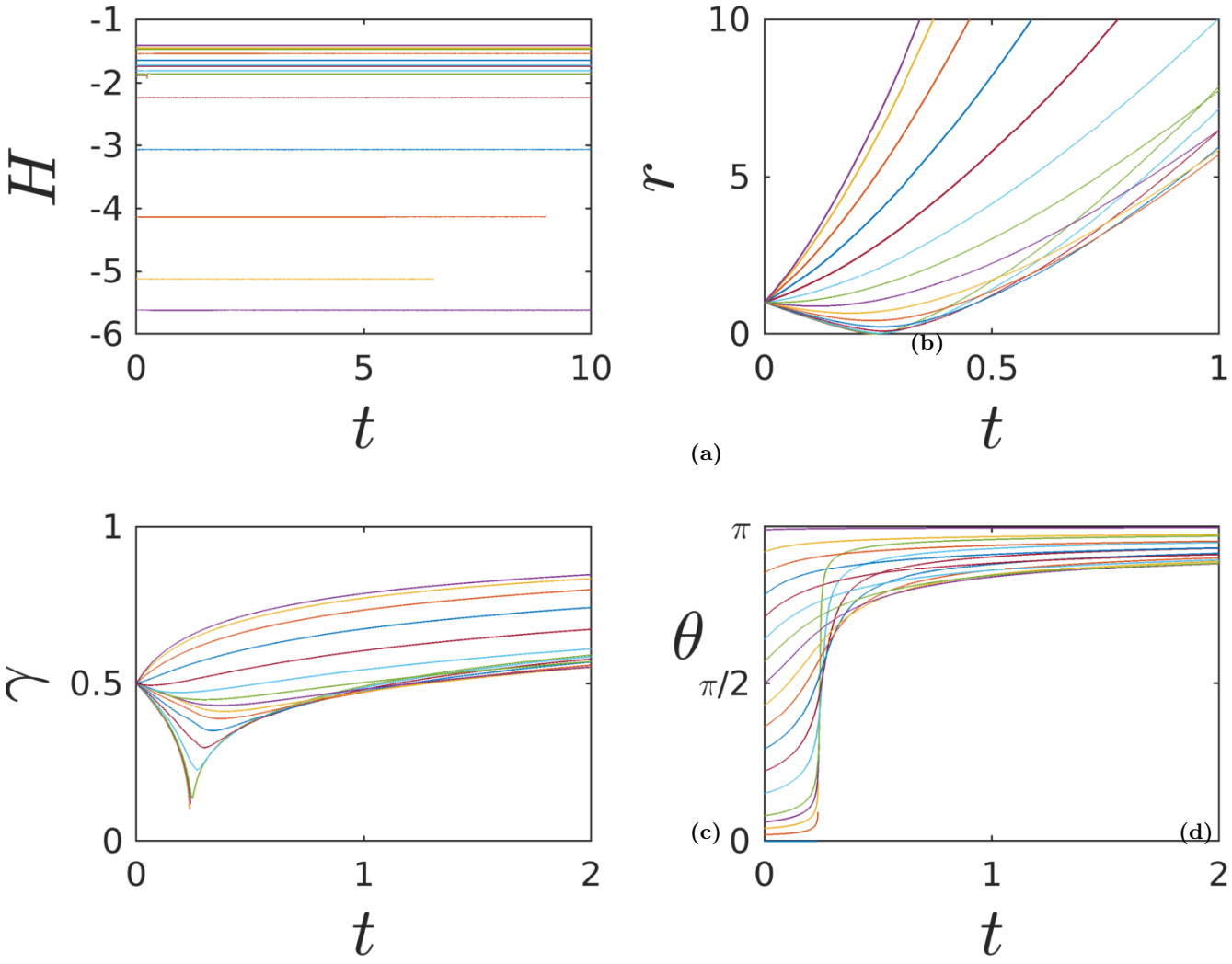

FIG. 4. Dynamics of a dipole of pinçons for various initial conditions. The radius is initially fixed to $r = 1$, the dipole intensity is initially set to $\gamma = 0.5$ and the initial dipole orientation is fixed at different values between 0 and π. The panel represent the time evolution of the different quantities: a) Hamiltonian; b) Distance between the two pinçons ; c) Dipole intensity; d) Dipole orientation.

III. DISCUSSION

We have introduced a model of singularities of Navier-Stokes, named pinçons , that follow Hamiltonian dynamics, obtained by the condition that the velocity field around these singularities obeys locally Navier-Stokes equations. This model can be seen of a generalization of the vorton model of Novikov[1], that was derived for the Euler equations. When immersed in a regular field, the pinçons are further transported and sheared by the regular field, while applying a stress onto the regular field, that becomes dominant at a scale that is smaller than the Kolmogorov length. We have shown that a pinçon dipole is intrinsically repelling, since two pinçons of same intensity but opposite direction generically run away from each other. For initial orientation in the interval $[0, \pi/2]$, however, the runaway stage is preceded by a transient collapse following a power law scaling, with dipole radius tending to 0 like $(t_c - t)^{0.63}$.

These solutions may prove of great interest from the point of view of the construction of weak solutions of the Navier-Stokes equations, in parallel to the effort done for the Euler equation [6]. Indeed, the Hamiltonian structure spares us the "gluing step" involved in the Mikado construction. Instead, it can be replaced by straightforward integration of ordinary partial differential equations, that allows to describe the dynamics of pinçon compatible with Navier-Stokes equations.

From another point of view, the pinçons dynamics is also reminiscent of the two fluid model of superfluid, where

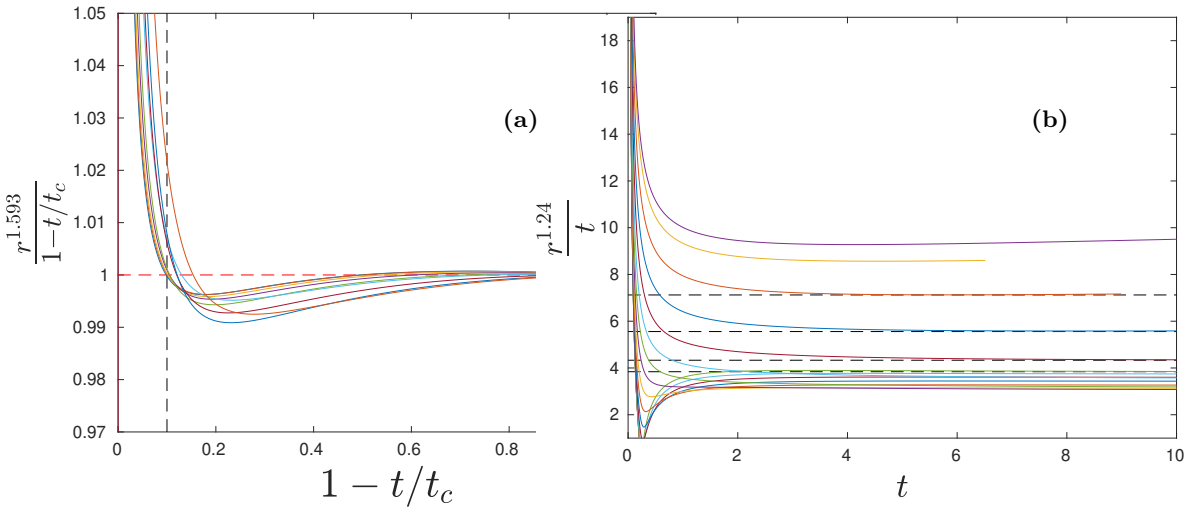

FIG. 5. Scaling law for the dipole separation. (a) Pre-collapse stage, for initial dipole orientation close to $\theta = 0$. We observe a power law behaviour, with exponent $r \sim (t_c - t)^{0.63}$; (b) Runaway stage, for long time. We observe a power law behaviour, with exponent $r \sim (t)^{0.81}$;

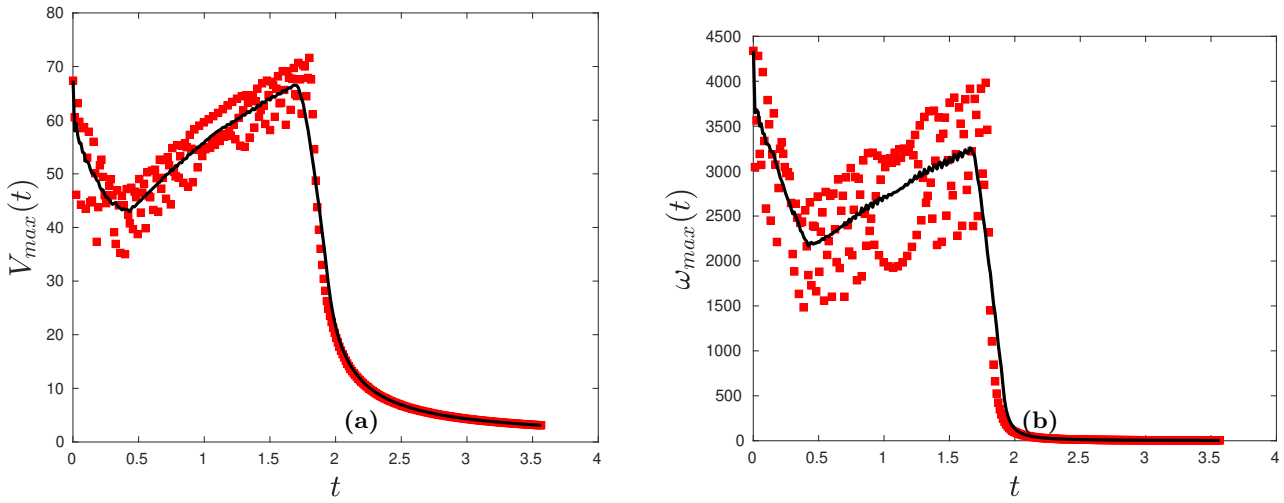

FIG. 6. Time evolution of the maximum of (a) Velocity and (b) vorticity field around a dipole with initial orientation $\theta_0 = \frac{\pi}{3} \in [0, \pi/2]$. The line is a moving average over 30 time steps.

the "regular" field, made of phonons, interact with the local topological defects that form the quantized vortices. However, as shown by [22], the interaction of quantized vortices leads to Leray scaling, with distance between vortices decaying like $\sqrt{t_c - t}$.

Finally, the description of the interaction between pinçons and a regular field is parallel to the interaction of localized wave packets interacting with a mean flow, in the WKB-RDT model of [25]. By analogy, one may then wonder whether it would be possible to use the pinçons as a subgrid scale model of turbulence, allowing to describe the interaction of a velocity field filtered at the Kolmogorov length, with a collection of pinçons that encode the very intense energy transfers that are observed when scanning very small scales of turbulence [].

Such a model would enable the use of larger time-steps, as the motion of the small scale motions is governed by Lagrangian motions. Further simplifications could also be obtained if one succeeds to do statistical mechanics of the pinçons , using their Hamiltonian dynamics. However, this is likely to be complicated, as the interactions are long-range, so that one can expect ensemble inequivalence, unless there is a screening mechanism similar to the Debye screening that limits the range of interactions. Another issue is whether a short range regularization is needed at short distances to make the model applicable to subgrid modelling.

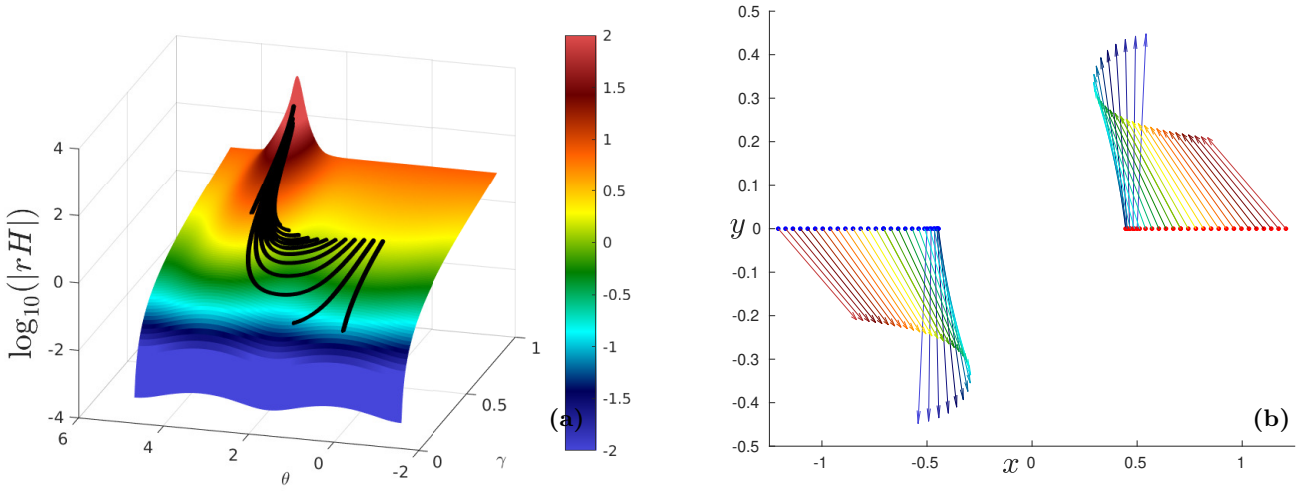

FIG. 7. (a) Behaviour of the solution along the hypersurface $H = H(t = 0)$. The plot represents the quantity $\log_{10}(|rH|)$, as a function of γ and θ. By construction, all dynamics occur onto the surface. Different trajectories corresponding to different initial conditions are materialized by black points. (b) Dipole dynamics as a function of time: the two points of the dipole (blue and red points) move initially towards each other until the dipole orientation is greater than $\pi/2$, in which case the dipole starts to run away at infinity, with axis becoming parallel to the dipole axis. The color of the vector codes the time, from $t = 0$ (dark blue) to $t = 1$ (dark red).

In any case, we hope the pinçons model will play a similar role than the Ising model in statistical mechanics, and stimulate new ideas regarding turbulence dynamics and properties.

[1] Novikov EA. 1983 Generalized dynamics of three-dimensional vortex singularities /vortons/. *Zhurnal Eksperimentalnoi i Teoreticheskoi Fiziki* **84**, 975–981.

[2] Gibbon JD, Pal N, Gupta A, Pandit R. 2016 Regularity criterion for solutions of the three-dimensional Cahn-Hilliard-Navier-Stokes equations and associated computations. *Phys. Rev. E* **94**, 063103.

[3] Constantin P, Weinan E, Titi ES. 1994 Onsager's conjecture on the energy conservation for solutions of Euler's equation. *Communications in Mathematical Physics* **165**, 207–209.

[4] Hicks W. 1899 Researches in vortex motion. Part III. On spiral or gyrostatic vortex aggregates. *Proceedings of the Royal Society of London* **62**, 379387.

[5] Constantin P, Majda A. 1988 The Beltrami spectrum for incompressible fluid flows. *Communications in Mathematical Physics* **115**, 435–456.

[6] Buckmaster T, De Lellis C, Székelyhidi L, Vicol V. 2018 Onsager's Conjecture for Admissible Weak Solutions. *Communications on Pure and Applied Mathematics* **72**, 229–274.

[7] Lundgren TS. 1982 Strained spiral vortex model for turbulent fine structure. *The Physics of Fluids* **25**, 2193–2203.

[8] Gilbert AD. 1993 A cascade interpretation of Lundgren stretched spiral vortex model for turbulent fine structure. *Physics of Fluids A: Fluid Dynamics* **5**, 2831–2834.

[9] Chorin AJ. 1991 Equilibrium statistics of a vortex filament with applications. *Comm. Math. Phys.* **141**, 619–631.

[10] Aksman MJ, Novikov EA, Orszag SA. 1985 Vorton Method in Three-Dimensional Hydrodynamics. *Phys. Rev. Lett.* **54**, 2410–2413.

[11] Alkemade AJQ, Nieuwstadt FTM, van Groesen E. 1993 The vorton method. *Applied Scientific Research* **51**, 3–7.

[12] Pedrizzetti G. 1992 Insight into singular vortex flows. *Fluid Dynamics Research* **10**, 101–115.

[13] Eyink GL. 2007-2008 Turbulence Theory. http://www.ams.jhu.edu/ eyink/Turbulence/notes/. course notes, The Johns Hopkins University,.

[14] Landau LD. 1944 A new exact solution of the Navier-Stokes equations. *Dokl. Akad. Nauk SSSR* **44**, 311314.

[15] Batchelor G. 2000 . In *An introduction to Fluid Dynamics*. Cambridge University Press.

[16] Tian G, Xin Z. 1998 One-point singular solutions to the Navier-Stokes equations. *Topol. Methods Nonlinear Anal.* **11**, 135–145.

[17] Cannone M, Karch G. 2004 Smooth or singular solutions to the Navier-Stokes system ?. *Journal of Differential Equations* **197**, 247–274.

[18] Sverák V. 2011 On Landau's solutions of the Navier–Stokes equations. *Journal of Mathematical Sciences* **179**, 208.
[19] Kruskal MD. 1974 The Korteweg-de Vries equation and related evolution equations. In *In: Nonlinear wave motion. (A75-14987 04-70) Providence* pp. 61–83.
[20] Calogero F. 1978 Motion of poles and zeros of special solutions of nonlinear and linear partial differential equations and related solvablemany-body problems. *Il Nuovo Cimento B (1971-1996)* **43**, 177–241.
[21] Calogero F. 2001 Classical many-body problems amenable to exact treatments. In *Lecture Notes in Physics* vol. 66. Springer Berlin.
[22] Villois A, Proment D, Krstulovic G. 2020 Irreversible Dynamics of Vortex Reconnections in Quantum Fluids. *Phys. Rev. Lett.* **125**, 164501.
[23] Leray J. 1934 Sur le mouvement d'un liquide visqueux emplissant l'espace. *Acta Math.* **63**, 193248.
[24] Yao J, Hussain F. 2020 On singularity formation via viscous vortex reconnection. *Journal of Fluid Mechanics* **888**, R2.
[25] Laval JP, Dubrulle B, Nazarenko S. 2004 Fast numerical simulations of 2D turbulence using a dynamic model for subfilter motions. *Journal of Computational Physics* **196**, 184–207.

IV. APPENDIX

A. Useful properties

We introduce the function: $\phi(\mathbf{x},\gamma) = \|\mathbf{x}\| - \gamma\cdot\mathbf{x}$. Such function has the properties:

$$\nabla_{\mathbf{x}}\phi = \frac{\mathbf{x}}{\|\mathbf{x}\|} - \gamma, \tag{34}$$

$$\phi = \mathbf{x}\cdot\nabla_{\mathbf{x}}\phi, \tag{35}$$

$$\nabla_{\gamma}\phi = -\mathbf{x}, \tag{36}$$

$$\Delta_{\mathbf{x}}(\ln(\phi)) = \frac{1-\gamma^2}{\phi^2}. \tag{37}$$

Therefore, $\mathbf{v}_\alpha$ can also be written:

$$\mathbf{v}_\alpha = -2\nabla(\ln\phi_\alpha) + 2\mathbf{x}\Delta\ln(\phi_\alpha). \tag{38}$$

With such expression, it is easy to check that $\mathbf{v}_\alpha$ is of zero divergence everywhere except at $x = 0$, where it is undefined.

B. Computation of the generalized momentum

By definition:

$$\mathbf{\Pi}_\alpha = \frac{1}{4\pi}\oint_{S_{\mathbf{x}_\alpha}} \mathbf{v}_\alpha \mathrm{d}S, \tag{39}$$

where $S_{\mathbf{x}_\alpha}$ is a sphere of center $\mathbf{x}_\alpha$, and of radius unity, and the integration is perform only over the surface of the sphere. Taking spherical coordinate system with respect to a vertical axis along $\boldsymbol{\gamma}_\alpha$, $\mathbf{x}-\mathbf{x}_\alpha = (\cos\psi\sin\theta, \sin\psi\sin\theta, \cos\theta)$, it is easy to see that the azimutal average of $\mathbf{x}-\mathbf{x}_\alpha$ perpendicular to $\boldsymbol{\gamma}_\alpha$ is zero, and that the only nonzero component is along $\boldsymbol{\gamma}_\alpha$, and gives $\langle\mathbf{x}-\ \mathbf{x}_\alpha\rangle_\psi = (0,0,\cos\theta)$. Using the fact that $\cos\theta = (1-\phi_\alpha)/\gamma$ with $\gamma = \|\boldsymbol{\gamma}_\alpha\|$, we thus get the azimutal average of $\mathbf{v}_\alpha$ as

$$\begin{aligned}\langle\mathbf{v}_\alpha\rangle_\psi &= (0,0,C),\\ C &= \frac{2\gamma}{\phi} - \frac{2(1-\phi)}{\gamma\phi} + 2\frac{(1-\gamma^2)(1-\phi)}{\gamma\phi^2},\end{aligned}$$

where we have dropped the subscripts α for simplicity. We may easily compute the integration of the various term over θ since after a change of variable $y = \cos\theta$, and we get for any $n \geq 0$

$$\begin{aligned}\langle\frac{1}{\phi^{n+1}}\rangle_\theta &= \int\frac{\sin\theta}{\phi^{n+1}}\mathrm{d}\theta,\\ &= \int_{-1}^{1}\frac{\mathrm{d}y}{(1-\gamma x)^{n+1}},\\ &= \frac{1}{n\gamma}\left(\frac{1}{(1-\gamma)^n} - \frac{1}{(1+\gamma)^n}\right),\end{aligned}$$

with the convention that $1/nx^n = \ln(x)$ when $n = 0$. Summing all the terms, we finally obtain equation 18.

C. Vorton dynamics

The dynamics of the vortons is given by [1]:

$$\dot{\mathbf{x}}_\alpha = -\frac{1}{4\pi}\sum_{\beta\neq\alpha}\frac{\mathbf{r}_{\alpha\beta}\times\boldsymbol{\gamma}_\beta}{\|\mathbf{r}_{\alpha\beta}\|^3}, \tag{40}$$

$$\dot{\boldsymbol{\gamma}}_\alpha = -\frac{1}{4\pi}\sum_{\beta\neq\alpha}\left[\frac{\boldsymbol{\gamma}_\alpha\times\boldsymbol{\gamma}_\beta}{\|\mathbf{r}_{\alpha\beta}\|^3} - 3\left(\boldsymbol{\gamma}_\alpha\cdot\mathbf{r}_{\alpha\beta}\right)\frac{\left(\mathbf{r}_{\alpha\beta}\times\boldsymbol{\gamma}_\beta\right)}{\|\mathbf{r}_{\alpha\beta}\|^5}\right]. \tag{41}$$